Chaos

Numerical experiments on quantum chaotic billiards

Cite as: Chaos **17**, 023116 (2007); https://doi.org/10.1063/1.2731307
Submitted: 07 November 2006 . Accepted: 26 March 2007 . Published Online: 21 May 2007

D. D. de Menezes, M. Jar e Silva, and F. M. de Aguiar


View Online


Export Citation

ARTICLES YOU MAY BE INTERESTED IN

Quantum mushroom billiards
Chaos: An Interdisciplinary Journal of Nonlinear Science **17**, 043125 (2007); https://doi.org/10.1063/1.2816946

Billiard dynamics: An updated survey with the emphasis on open problems
Chaos: An Interdisciplinary Journal of Nonlinear Science **22**, 026116 (2012); https://doi.org/10.1063/1.4729307

Expansion method for stationary states of quantum billiards
American Journal of Physics **67**, 133 (1999); https://doi.org/10.1119/1.19208

AIP Publishing

© 2007 American Institute of Physics.

Numerical experiments on quantum chaotic billiards

D. D. de Menezes, M. Jar e Silva, and F. M. de Aguiar[a)]
Departamento de Física, Universidade Federal de Pernambuco, Recife, PE 50670-901, Brazil

(Received 7 November 2006; accepted 26 March 2007; published online 21 May 2007)

A recently proposed numerical technique for generation of high-quality unstructured meshes is combined with a finite-element method to solve the Helmholtz equation that describes the quantum mechanics of a particle confined in two-dimensional cavities. Different shapes are treated on equal footing, including Sinai, stadium, annular, threefold symmetric, mushroom, cardioid, triangle, and coupled billiards. The results are shown to be in excellent agreement with available measurements in flat microwave resonator counterparts with nonintegrable geometries. © *2007 American Institute of Physics*. [DOI: 10.1063/1.2731307]

Signatures of chaos have been intensively searched in quantum mechanics during the past two decades. Whatever they are, these elusive chaotic features might be expected to show up only in the highly excited states of a quantum system, which are typically hard to calculate and of difficult experimental access. Perhaps the most convenient and simplest tool to tackle the issue of chaos in quantum dynamics is a *billiard*. In classical billiards (CBs), one investigates the trajectories traced by a frictionless point mass as it moves across a plane and elastically scatters off the hard boundary of a closed planar domain. In other words, CBs are Hamiltonian systems that can exhibit a completely regular (integrable) behavior, a completely chaotic (nonintegrable) dynamics, or something in between (a divided phase space), depending on its geometry. There is a vast literature on CBs in both physical and mathematical communities. In the quantum limit, we have a problem of a particle confined in a two-dimensional cavity, whose wave function obeys the Helmholtz equation. The same equation describes the classical electrodynamics of TM microwave modes in a flat resonator, which leaves room for experimental investigations of quantum billiards, in addition to the opportunities of analytical and numerical studies. Since there are no explicit formulas for the solution of such a boundary-value problem when the classical limit is chaotic (or mixed), the need for accessible and efficient codes to solve the Helmholtz equation is rampant. There are currently numerous methods for that purpose. In this paper, a recent numerical technique is applied broadly to provide an overview of eigenfunctions and eigenvalues in some of the most important quantum chaotic billiards hitherto studied in the literature. When possible, a comparison is given between our numerical results and those from physical experiments in microwave billiards, and those obtained with other numerical methods as well.

In the past two decades, two-dimensional cavities have been extensively used as model systems in the study of quantum mechanics where the classical description yields chaotic dynamics.[1] Earlier theoretical studies in the 1970s were mainly concerned with the eigenvalues (EVs) of nonintegrable systems. In particular, the role of periodic orbits in the theory of semiclassical quantization of bound states attracted much interest. In the mid-1980s, Bohigas, Giannoni, and Schmit[2] have found numerically that the energy-level fluctuations of a "desymmetrized" Sinai billiard exhibit universal properties consistent with the predictions of random matrix theory.[3] Soon after, Heller[4] addressed the effect of unstable periodic orbits on the eigenfunctions (EFs) of classical chaotic systems. These advances on the theoretical side strongly demanded experimental tests of a number of predictions and conjectures. Since the early 1990s, different cavity-based systems have been used to characterize experimentally the so-called quantum or wave chaology, including flat microwave cavities,[5–7] electron quantum dots,[8] ultracold atoms,[9] vertical cavity surface emitting lasers,[10] water vessels,[11] vibrating blocks,[12] and quantum corrals.[13]

As an advantage, flat microwave cavities with perfectly conducting walls enjoy a simple equivalent quantum analog, namely a single particle (mass m) confined in a two-dimensional infinite quantum well. In both systems, the time-independent factor of the underlying wave function is a solution of the Helmholtz equation

$$(\nabla^2 + k^2)F(x,y) = 0, \tag{1}$$

with Dirichlet boundary condition $F=0$ at the contour of the confining cell. In the quantum case, $k=(2m\varepsilon)^{1/2}/\hbar$, $\hbar$ is Planck's constant, and ε is the energy EV. In the electromagnetic case, $k=2\pi f/c$, where f is the eigenfrequency and c is the speed of light. The function F is the electric field component perpendicular to the cavity plane, $E_z(x,y)$, associated with a transverse magnetic resonant mode. For a typical cavity thickness $d=0.6$ mm, the two-dimensional nature of the eigenmodes is guaranteed for frequencies below $c/2d \sim 25$ GHz. In fact, both normal and superconducting microwave resonators have been instrumental in testing a number of theoretical predictions in wave chaology in the past 15 years.

a)Electronic mail: fma@df.ufpe.br

 © 2007 American Institute of Physics

For a billiard of complicated shape, it may be nearly impossible to solve the eigenvalue problem posed by (1). Certain families of EVs and EFs of interior domains may be approximated using different analytical techniques including ray theory[14] and Green functions.[15] On the other hand, numerical approaches tend to be less restricted but may face severe difficulties in treating domains with reentrant corners and holes. Boundary methods,[16] which reduce the calculation of EVs and EFs to a problem involving the billiard contour only, the expansion method,[17] and the finite-element method (FEM),[18] are possible numerical techniques to solve (1) for a given geometry. The FEM is well established and has a broader range of applications. Recently,[19] a FEM[20] was used to study the statistics of higher-order EVs of a threefold symmetric billiard with a hole, for which a large hardware cluster system and several hours of CPU time have been employed. In some situations, simpler schemes might be desirable. Here, a user-friendly, public, and remarkably efficient mesh generator[21] is combined with a standard FEM[18] to solve (1) for both EVs and EFs of several quantum chaotic billiards. The results are shown to be in excellent agreement, to a desired precision, with physical experiments in microwave chaotic billiards. The geometries were primarily chosen from the *physical* experiments, namely Sinai,[6] stadium,[5(b)] and annular[22] billiards. In addition, we provide results for some EFs corresponding to threefold symmetric billiards whose spectra were recently studied experimentally in Ref. 23 and numerically in Ref. 19. We then discuss the issue of quantum localization in two coupled Sinai billiards. Finally, in the last paragraph, we apply the method to other geometries recently investigated, namely, the mushroom, cardioid and irrational triangular billiards. The numerical results provided here were calculated in a single computer with a 2.2-GHz processor and 2 gigabytes of random access memory. With this configuration, the needed CPU time T is typically a few seconds for 100 EVs and corresponding EFs, if one uses a number of nodes $N \sim 1000$ in the discretization mesh. In this case, the precision is certainly reduced, but the pattern of nodal lines obtained might be quite satisfactory for a quick crosschecking with results from physical experiments, particularly for the low-lying eigenstates. T grows polynomially (up to N^3) for a given set of numerical parameters, and may reach a few hours for a precise computation of higher-order solutions. We briefly describe the method below, and selected results, both numerical and physical, are then presented and compared in what follows.

Mesh generation. The FEM numerically approximate the solution of a partial differential equation by replacing the continuous system with a finite number of coupled algebraic equations. These equations result from the discretization of the interior domain D (two-dimensional here) by small elements (typically triangles), whose boundaries form a mesh within D. Generating a mesh is thus the first key step in a FEM. A high-quality mesh with triangular elements must have triangles that are nearly equilateral to provide a well conditioned system of algebraic equations. A number of mesh generation algorithms have been developed in the past decades. Almost always, these algorithms are codes with difficult access, if any. A recent exception is the mesh generator proposed in Ref. 21 by Persson and co-workers, which uses a *signed distance function* to represent the geometry, a *force-displacement function* to move the nodes in the mesh, and a standard (Delaunay) triangulation algorithm to dynamically adjust the topology until a mesh of high quality is obtained. Thus, for a given hardware, the resulting CPU time T basically depends on the mesh quality required, the number N of nodes in the mesh needed for a given precision, and the number of eigensolutions to be investigated. The method can easily handle domains with a hole. Refinement around corners or other complicated boundaries is just an option to a uniform mesh in the algorithm provided in Ref. 21. Both EVs and EFs can be obtained with suitable commands of the commercial software MATLAB, a very useful tool in dealing with the underlying sparse matrices. For instance, the calculation of n EVs, the smallest ones or the ones closest to a given number, and corresponding EFs, is done with the function "*eigs*," which calls the appropriate solver package.

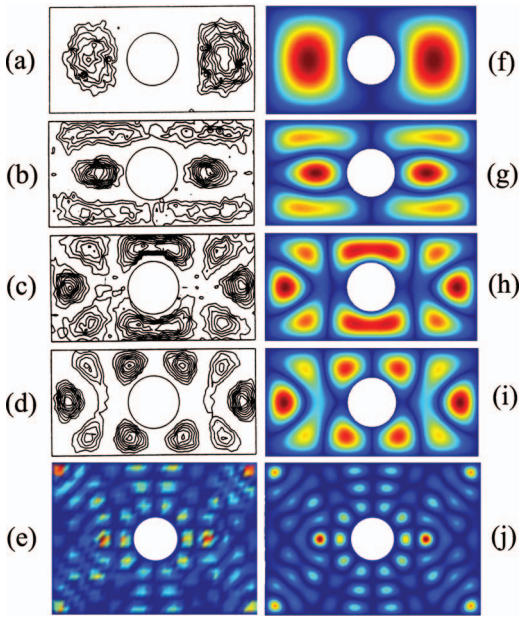

FIG. 1. (Color) Standing-wave patterns in Sinai billiards. (a)–(d) are microwave measurements by Sridhar and co-workers [adapted from Ref. 6(b)]. (e) is an experimental result in another microwave billiard, by the authors. (f)–(j) are the corresponding numerically calculated eigenfunctions. Parameters are given in the text.

Sinai billiards. A Sinai billiard is geometrically defined by a double boundary composed by an outer rectangle of lateral dimensions ℓ and d, and an inner concentric circle of radius r. Three room-temperature microwave experiments are addressed here. Two of them have been made previously by Sridhar and co-workers[6] and the other one was carried out recently in our own microwave laboratory. They share the same perturbation measurement technique, described in detail in Ref. 6(b), and they differ in the geometric parameters used. Tens of the lowest-lying EFs of a billiard with $\ell = 44.0$ cm, $d = 21.9$ cm, and $r = 5.00$ cm have been measured in Ref. 6(b); four of them are reproduced here by the contour plots (a)–(d) of Fig. 1. The measured frequencies in GHz are 1.082 (a), 2.181 (b), 2.373 (c), and 2.446 (d). We have solved (1) for this geometry for the 100 lowest-lying EVs and EFs with $N = 25741$ nodes (ca. 60000 triangular elements) and a resulting $T \sim 10$ min. Density plots of the numerically calculated $|E_z(x,y)|$ with eigenfrequencies 1.082, 2.194, 2.363,

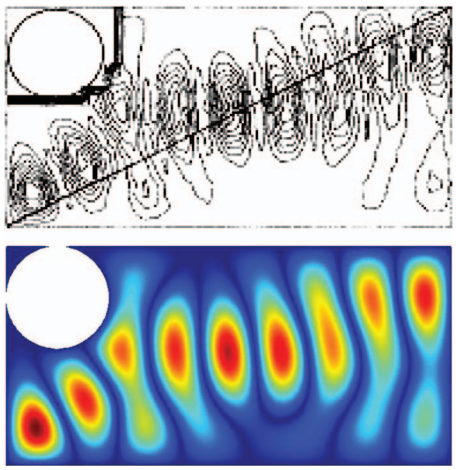

FIG. 2. (Color) Diagonally scarred eigenfunction in a Sinai-type billiard. Upper panel: Microwave experiments by Sridhar [Ref. 6(a)]. The measured frequency is 3.138 GHz. Lower panel: Density plot of the numerically calculated $|E_z(x,y)|$ for the corresponding eigenstate at 3.143 GHz.

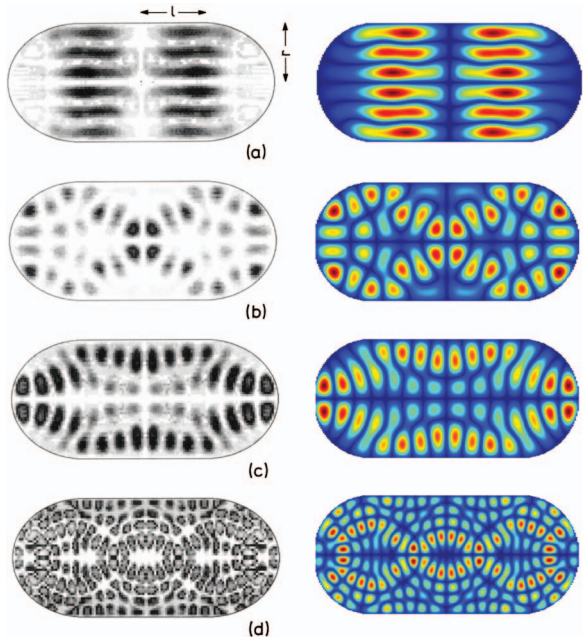

FIG. 3. (Color) Left panels: Measured eigenstates in a microwave stadium billiard by Stein and Stöckmann [Ref. 5(b)], with $\ell=18$ cm and $r=13.5$ cm. From top to bottom, the measured eigenfrequencies are 3.384, 3.865, 4.056, and 7.250 GHz. Right panels: Density plots of the calculated $|E_z(x,y)|$ of the corresponding resonances with frequencies 3.393, 3.847, 4.066, and 7.277, from top to bottom, respectively.

and 2.483 GHz are shown in panels (f), (g), (h), and (i), respectively. A negligible difference between the measured and the calculated EVs is observed for these low-lying eigenstates, given the experimental uncertainties, including tiny frequency shifts due to the small input and output antennae used in the transmission experiments. It is worth noting that the features discussed in Ref. 6(b) concerning accidental near-degeneracy of the EFs are also observed in the numerical results. The measurements in our laboratory were made at room temperature in a Cu Sinai billiard with $\ell=41.0$ cm, $d=29.0$ cm, and $r=5.00$ cm. Panel (e) in Fig. 1 shows the measured higher-order mode with eigenfrequency 5.200 GHz. The corresponding EF was calculated at 5.207 GHz and is shown in panel (j) of Fig. 1, again in excellent agreement with the experimental result. In order to illustrate the effectiveness of the numerical method used here, we reproduce in the upper panel of Fig. 2 a measurement reported in Ref. 6(a) for a configuration then regarded as "difficult to study using purely numerical methods." The nominal values provided in Ref. 6(a) are $\ell=44.0$ cm, $d=21.8$ cm, and $2r=10.15$ cm. The corresponding numerically calculated EF is shown by the density plot in the lower panel of Fig. 2. Both results show the same diagonally scarred pattern, with a measured frequency of 3.138 GHz and a calculated one of 3.143 GHz, in good agreement.

Stadium billiard. Another prototype chaotic billiard is the stadium, whose single contour is comprised of two parallel segments, each with length 2ℓ, separated by a distance $2r$, and bracketed by the two halves of the circumference of radius r. We focus here on the room-temperature reflection experiments by Stein and Stöckmann,[5(b)] in which a single mobile antenna was used to measure the microwave field distribution. The left panels in Fig. 3 were taken from Ref. 5(b) and correspond to twofold reflection of measurements in a quartered stadium billiard with $\ell=18$ cm and $r=13.5$ cm. The calculated EFs displayed on the right panels in Fig. 5 were obtained with $N=44612$ and $T\sim 30$ min. Again, a good quantitative agreement between the microwave and numerical experiments is achieved. Notice that the higher the level orders, the smaller the mean level spacing. Thus, a better precision might be required to find among the calculated modes the one corresponding to a given measurement. We stress that with the precision used in this case, the higher-order mode corresponding to the measured eigenfrequency of 7.250 GHz could easily be found among the ten calculated nearest neighbors to that frequency.

Annular billiard. The successful numerical tests presented above have drawn our attention to other billiards recently investigated experimentally by Richter and co-workers,[22,23] with superconducting microwave cavities at cryogenic temperatures. In this case, quality factors of 10^6 may be reached, allowing the measurement of high-resolution spectra. We address first the annular billiard studied in Ref. 22, where evidence for chaos-assisted tunneling has been observed experimentally for the first time. The double boundary of the annular billiard is defined by two circumferences, with radius r (inner circle) and R (outer circle), and an eccentricity δ. The experiments in Ref. 22 were carried out with a nominal value $R=12.5$ cm and three different configurations of the family $r+\delta=0.75R$. Here we focus on the configuration with $\delta=2.5$ cm ($r=6.875$ cm). The three upper panels in Fig. 4, taken from Ref. 22, correspond to *room-temperature* measurements of three resonant modes in a copper annular billiard. They have been identified by broad peaks observed in the transmission spectrum, nearly centered at 8.912, 8.927, and 8.942 GHz, from left to right in the upper panels of Fig. 4, respectively. The middle eigenstate actually corresponds to the even-parity member of a quasidoublet of whispering gallery modes, as suggested in Ref. 22 by a high-resolution spectrum of a niobium superconducting billiard with the same shape. For these low-temperature (4.2 K) experiments, the three resonance frequencies are actually shifted, as shown by the sharp peaks in the spectrum of the inset of the

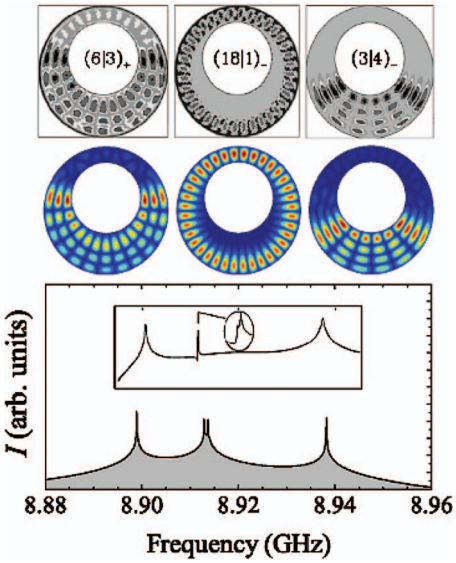

FIG. 4. (Color) Top three panels: Measured eigenstates in a Cu annular microwave billiard at room temperature (Ref. 22). The measured frequencies are, from left to right, close to 8.912, 8.927, and 8.942 GHz, respectively. Middle panels: Calculated EFs corresponding to the three resonances shown in the shaded spectrum of the lower panel. Inset: Measured spectrum at 4.2 K in a superconducting Nb cavity with the same shape as the Cu billiard (Ref. 22).

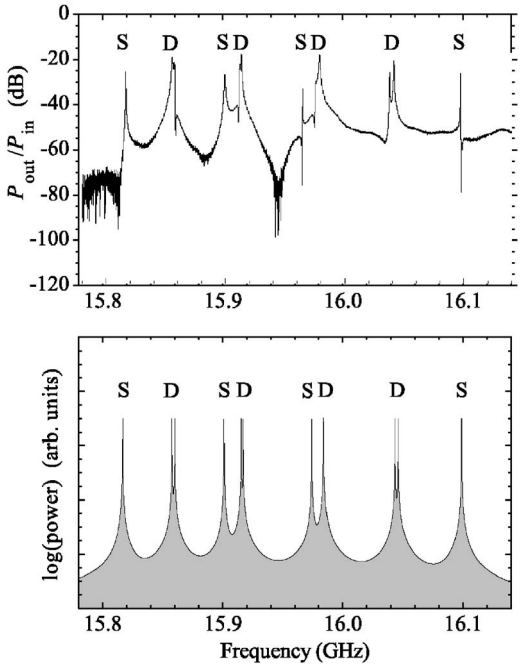

FIG. 5. Upper panel: Higher-order resonances in the measured spectrum of a chaotic superconducting microwave billiard with threefold symmetry, taken from Ref. 23(b). Lower panel: Numerically calculated spectrum in the same frequency range. S and D stand for singlet and doublet, respectively.

lower panel in Fig. 4, also taken from Ref. 22. These small displacements were attributed to mechanical imperfections and positioning errors of the inner circles within the resonators.[22] Here we offer an estimate of the mechanical and positioning uncertainties for the low-temperature measurement. By trial and error, using a relatively low precision, we varied the values of the parameters r, R, and δ until a singlet-doublet-singlet sequence occurred in the [8.88 GHz, 8.96 GHz] measurement interval. A few fine tunings at higher precision led to the shaded spectrum in the bottom panel in Fig. 4, obtained with $N=62307$ nodes, $T\sim 1.5$ h, and a visual optimization such that, for all peaks shown in the experimental spectrum,[22] the absolute value of the difference between the calculated and the experimental frequencies was smaller than $\Delta f/4$, where $\Delta f=0.02$ GHz is the scale provided in Ref. 22. The spectrum is comprised of Lorentzian curves[24] centered at the numerically calculated eigenfrequencies with arbitrary linewidths, just to mimic the experimental result. The parameters used were $R=12.5432$ cm, $r=6.886$ cm, and $\delta=2.510$ cm, slightly different with respect to the nominal experimental values. The three middle panels in Fig. 4 are the corresponding density plots of the calculated $|E_z(x,y)|$ for each eigenstate. The close similarity with the upper panels confirms that the displaced peaks at low temperature indeed correspond to the same three eigenmodes measured at room temperature.

Threefold symmetric billiards. Based on the group-theoretic concept of structural invariance, Leyvraz, Schmit, and Seligman[25] predicted that time-reversal invariant systems may have invariant subspaces on which the spectrum exhibits fluctuations characteristic of systems without time reversal symmetry, i.e., those of the Gaussian Unitary Ensemble (GUE).[3] The analytical results were further tested numerically in Ref. 25 through a billiard with threefold symmetry. Quantum mechanically, such billiards have three classes of EFs (three invariant subspaces), according to the angular momentum ($m_\ell=0,\pm 1$). A rotation of 120° about the quantization axis introduces a phase factor $\exp(2m_\ell\pi i/3)$ in the EF with quantum number m_ℓ, and the states with $m_\ell=\pm 1$ are degenerate due to time-reversal (complex conjugation) invariance. Thus, the spectrum of the billiard is comprised of threefold symmetric singlets and spatially asymmetric doublets. Confirming experimentally this numerically tested theoretical prediction, Richter and co-workers[23] investigated the level statistics of a fully chaotic triangular microwave billiard, whose single boundary is parametrized in polar coordinates by[23(a)]

$$r(\phi)=r_0[1+0.2\cos(3\phi)-0.2\sin(6\phi)]. \quad (2)$$

Singlets and doublets were then elegantly identified in high-resolution experiments[24] through a phase-shift double input technique. Part of the measured transmission spectrum is reproduced here in the upper panel of Fig. 5, where S and D stand for singlet and doublet, respectively. The lower panel is a visually optimized spectrum, calculated with $N=139483$ nodes and $T\sim 3$ h. As in Fig. 4, the resonances are Lorentzians centered at the calculated eigenfrequencies. Guided by a 100-mm bar provided in Ref. 23, we first estimated a value for the parameter r_0 at a lower numerical precision. A few attempts at higher precision yielded the shaded spectrum in Fig. 5, obtained with $r_0=9.614$ cm. The room-temperature experimental value is 9.62 cm.[26] Since this value shrinks slightly at lower temperatures, the agreement between the experimental and the numerically obtained values is remarkable. The EFs of this billiard were not measured in Ref. 23 and we offer here in Fig. 6 the calculated threefold symmetric singlets in the spectrum of Fig. 5.

Triangular billiards with holes. As a sidelight to the previous presentation of comparative studies between physical

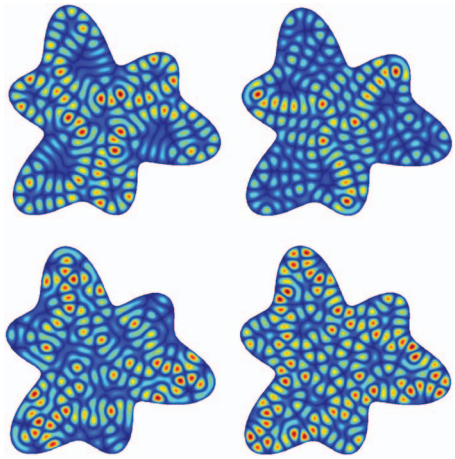

FIG. 6. (Color) Numerical results, showing density plots of $|E_z(x,y)|$ corresponding to the threefold symmetric singlet states in the lower spectrum of Fig. 5. The calculated eigenfrequencies are, left to right, 15.8167 and 15.9012 GHz for the upper panels, and 15.9741 and 16.0988 GHz for the lower panels.

and numerical experiments, we add now an application of the numerical method to *triangular* cavities with a hole, such as the one studied in Ref. 19. In this case, the interior domain of interest has outer and inner contours, as in the Sinai and annular billiards. These two boundaries are described, in polar coordinates, by the functions[19]

$$r_a(\phi) = r_{0a}[1 + 0.3\cos(3\phi)] \tag{3}$$

and

$$r_b(\phi) = r_{0b}\{1 + 0.1\cos[3(\phi + \alpha)]\}. \tag{4}$$

Both boundaries possess threefold symmetry and are rotated against each other by an angle α. Equations (3) and (4) were introduced in Ref. 19, where the EVs of billiards with the outer boundary given by (3) with $r_{0a}=10.000$ cm, and the inner one by (4) with $r_{0b}=2.727$ cm, were numerically calculated for three different values of the angle α. Confirming earlier theoretical predictions and numerical tests,[25] the authors in Ref. 19 have successfully tested a numerical approach[20] by showing that a transition from GOE to GUE statistics[3] occurs in the spectrum of the billiard as α is changed from 0° (C_{3v} symmetry) to 10° (C_3 symmetry). Billiards with a hole can be conveniently handled with the MATLAB function *ddiff*, as proposed in Ref. 21. We have introduced Eqs. (3) and (4) into this function and have been able to calculate the EVs and EFs of a number of billiards based on these equations. The first five threefold symmetric singlet states of two of these billiards are reported here. The left panels in Fig. 7 correspond to the billiard studied in Ref. 19 with $\alpha=0°$. Assigning an integer number n ($n \geqslant 1$) to each state in the spectrum, starting from the ground state, these singlets correspond to $n=1$, 6, 7, 12, and 13, from top to bottom, respectively. The calculated frequencies are 2.0681, 3.1629, 3.2517, 3.9987, and 4.2917 GHz, also from top to bottom. The right panels in Fig. 7 correspond to a billiard in which the outer boundary is given by (4) with $r_{0b}=10.000$ cm, the inner contour is given by (3) with $r_{0a}=2.727$ cm, and $\alpha=0°$. In this case, the singlet states correspond to $n=1$, 6, 7, 12, and 15, and $f=2.1145$, 3.0669, 3.1238, 4.2982, and 4.5664 GHz, from top to bottom, respectively. In both cases, we have employed $N=35200$ nodes in the mesh, with a resulting CPU time $T \sim 10$ min.

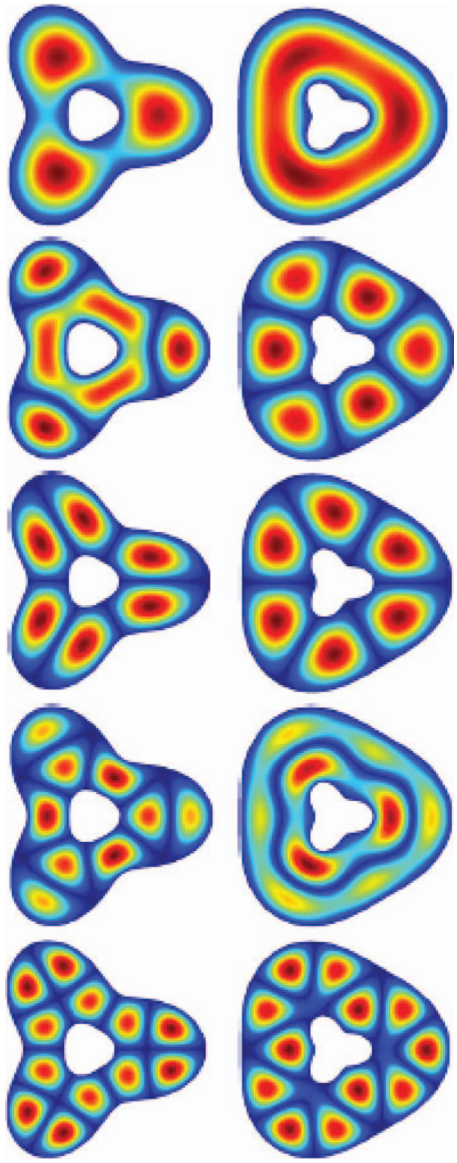

FIG. 7. (Color) Calculated standing wave patterns in threefold symmetric parametric billiards with holes, corresponding to the first five singlet eigenstates. Left panels: Outer and inner boundaries are given by (3) and (4), respectively, with $\alpha=0°$. Right panels: Outer and inner boundaries are given by (4) and (3), respectively, with $\alpha=0°$. Parameters are given in the text.

Two coupled Sinai billiards. Let us now consider the case of two identical Sinai billiards, each with $\ell=44.0$ cm, $d=21.9$ cm, and $r=5.00$ cm, as the one in Ref. 6(b) symmetrically connected through a narrow channel, 0.5 cm long and 2.0 cm wide. We used a mesh (Fig. 8) with $N=142151$ ($T \sim 3$ h). The ground state of one (uncoupled) such billiard has two partners with eigenfrequencies $f=1.081$ and 1.082 GHz, with even and odd parity with respect to the central vertical axis, respectively. In each mode, $|E_z(x,y)|^2$ has two local maxima, as shown in Figs. 1(a) and 1(f). As a result of parity, while the mode at 1.081 GHz has saddles at the bottleneck regions below and above the central circle, its partner at 1.082 GHz exhibits a nodal line at the central vertical axis [Fig. 1(f)]. In the coupled system, a quasiquadruplet is thus observed at $f=1.0778$, 1.0800, 1.0813, and 1.0814 GHz. The

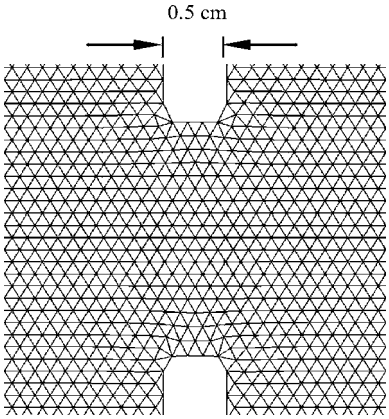

FIG. 8. Detail of the quasiuniform mesh used throughout the constriction to numerically solve the eigenvalue problem of two coupled Sinai billiards, as described in the text.

odd partners with $f=1.0800$ and 1.0814 GHz exhibit four maxima, one strong and one weak in each billiard. Strikingly, in the even modes with $f=1.0778$ and 1.0813 GHz, the weak extrema almost vanish. The resulting EFs are shown by the density plot in the two upper panels of Fig. 9. The same localization pattern occurs for other quasiquadruplets, such as those calculated at $f=7.9455$, 7.9456, 7.9460, and 7.9466 GHz, for instance. The corresponding standing-wave patterns of the first and third modes in that sequence are shown in the lower panels of Fig. 9. As in the ground state, the wave function is either strongly localized at the inner sectors of the billiard (lower f) or at the outer sectors (higher f). We refer to this localized standing-wave pattern as "type-II half-filling," in order to distinguish it from the more familiar situation of doublets due solely to symmetry. As in homonuclear diatomic molecules,[27] if two eigenmodes are degenerate, they resemble states of two distinguishable localized sites. Two of these states with, say, "type-I half-filling," are shown in Fig. 10 for the coupled billiard system. They correspond to a doublet calculated at 3.1077 GHz. Previously,[6(c)] type-II half-filling localization has been observed in microwave experiments in a single Sinai billiard, as a symmetry broken state due to a slightly displaced disk. Such a state was compared with a numerically calculated superposition of even-odd partners of the symmetric billiard. Even in this simpler situation, the relation between wave mechanics and the corresponding classical ray trajectories was not completely understood. Interesting states symmetrically distributed nearly over the entire system are shown in Fig. 11. The standing-wave pattern in the top panel of Fig. 11, observed at a resonance frequency $f=4.0214$ GHz, is reminiscent of the $TM_{10,3}$ mode in the bare uncoupled rectangular billiard, and the odd member of a quasidoublet. The other panels in Fig. 11 show kaleidoscopic modes at higher frequencies. Remarkable eigenstates of the coupled system that are also related with the issue of quantum localization are shown in Fig. 12. A common feature of these states is that they exhibit a relatively large peak in the wave intensity *at* the narrow channel, where the amplitude is often strongly suppressed. Notice that open-ended tube resonances might be expected only at $f\sim c/2\,L\sim 30$ GHz for a channel with length $L=0.5$ cm. On the other hand, for a width $W=2.0$ cm, transverse resonances might occur around $f=c/2W\sim 7.5$ GHz. The frequencies in Fig. 12 are close to this value, but their connection with W in this two-dimensional problem is nontrivial; for instance, localized

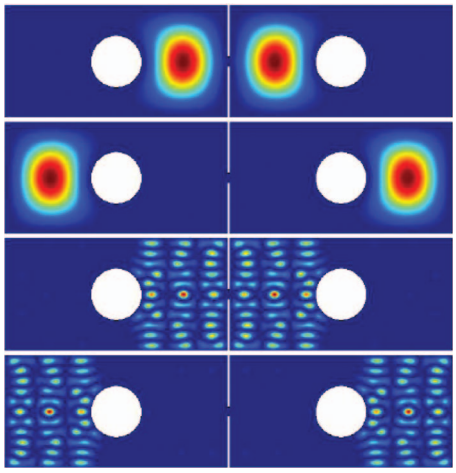

FIG. 9. (Color) "Type-II half-filling:" Localized modes in two coupled Sinai billiards. Each cell has the same dimensions as the billiard in Fig. 1(f). The coupling channel is 0.5 cm long and 2.0 cm wide. The calculated eigenfrequencies are 1.0778, 1.0813, 7.9455, and 7.9460 GHz, from top to bottom, respectively.

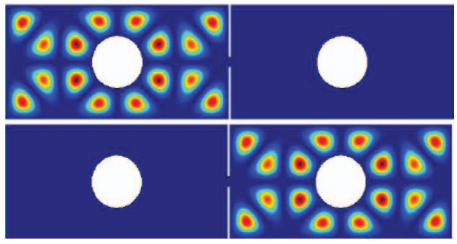

FIG. 10. (Color) "Type-I half-filling:" Localized modes in two coupled Sinai billiards, corresponding to a doublet with $f=3.1077$ GHz.

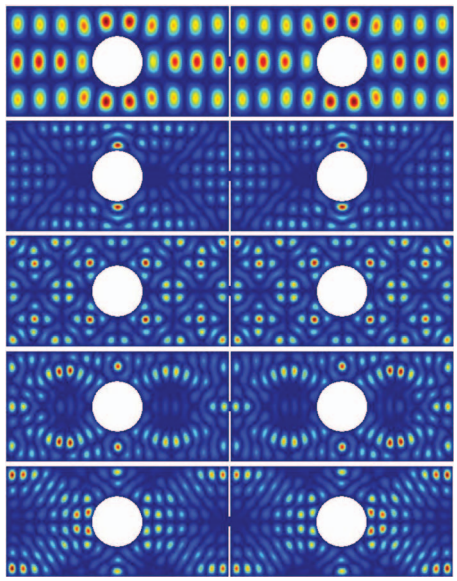

FIG. 11. (Color) Standing-wave patterns corresponding to extended states. From top to bottom, the calculated eigenfrequencies are 4.0214, 7.8566, 7.9790, 8.0816, and 8.1515 GHz, respectively.

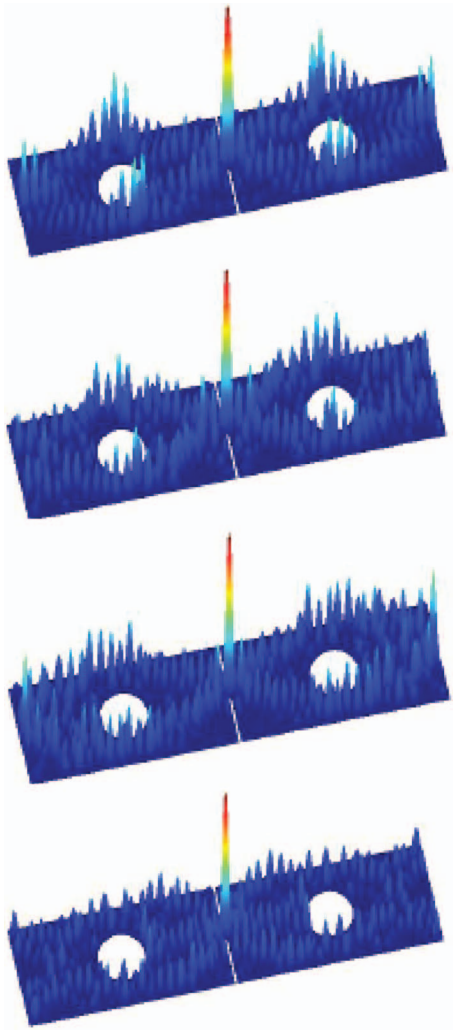

FIG. 12. (Color) Tridimensional plots of $|E_z(x,y)|^2$ for states strongly localized at the narrow channel coupling two identical Sinai billiards. From top to bottom, the calculated eigenfrequencies are 7.3521, 7.6631, 8.2744, and 8.4351 GHz, respectively.

modes such as those in Fig. 12 are also observed with frequencies between 8 and 9 GHz, i.e., well above $c/2W$. One important feature is shared by these localized wave functions, namely, the presence of a *scarr*[4] through the channel. It is worth noting that such localized states also occur in two coupled rectangular cavities. Here we consider the bare rect-

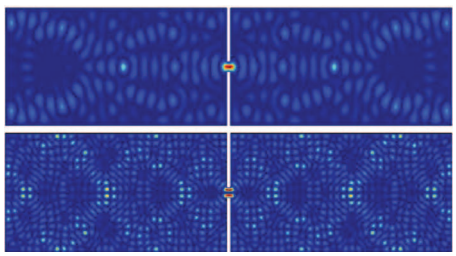

FIG. 13. (Color) Density plots of $|E_z(x,y)|^2$ for states strongly localized at the narrow channel coupling two identical rectangular billiards, with the same dimensions as those in Figs. 9–12. Upper panel: Eigenmode at $f=7.7317$ GHz, showing a single large peak at the constriction. Lower panel: Eigenmode at $f=15.5358$ GHz, with two large peaks on the coupling channel.

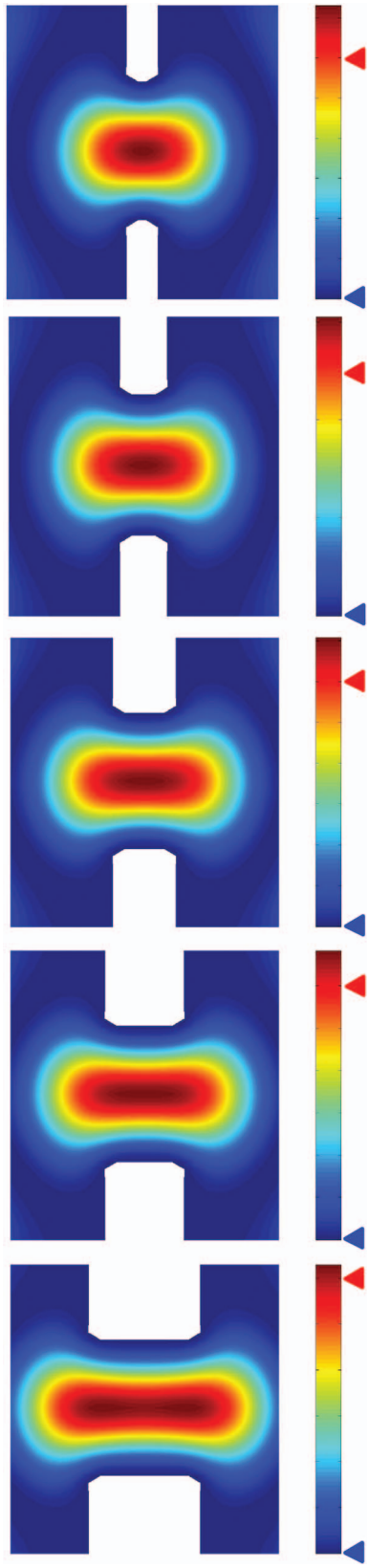

FIG. 14. (Color) Density plots of $|E_z(x,y)|^2$ in a 2 cm$\times$2 cm region centered at the narrow channel coupling two rectangular billiards. From top to bottom, the channel length is $L=0.42$, 0.620, 0.70, 0.86, 1.10, and 1.58 cm, respectively. The small triangles indicate the "0" and the "1" normalized intensity levels in the color bar. The standing-wave pattern in each rectangle pair is the same as that in the upper panel of Fig. 13. Frequencies are given in Fig. 15.

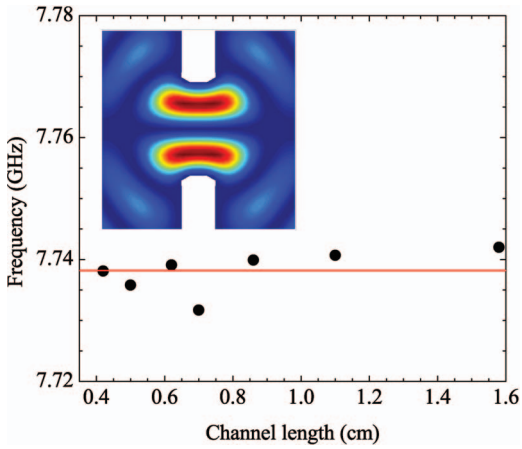

FIG. 15. (Color) Calculated eigenfrequency for the same eigenmode in two coupled rectangular billiards as a function of the length of the coupling channel (symbols). The horizontal line indicates the average frequency. Inset: Density plots of $|E_z(x,y)|^2$ in a 2 cm$\times$2 cm region centered at the narrow channel, corresponding to the eigenmode at 15.5358 GHz shown in the lower panel of Fig. 13.

angles corresponding to the above Sinai billiards (ℓ =44.0 cm, d=21.9 cm), coupled through the same narrow channel. Two modes strongly localized at the constriction are shown in Fig. 13 for this system, one with eigenfrequency around 7.5 GHz and the other one close to the second harmonic at 15 GHz. As in the coupled Sinai system, these localized modes are not unique. Other modes with a relatively large peak at the coupling channel are also observed in the coupled rectangular system in the 8–9 GHz interval. By fixing the number of nodes in the mesh ($N\sim$155000) and varying the channel length L, we have followed a mode with a well defined standing-wave pattern, namely, that in the upper panel of Fig. 13. Figure 14 shows density plots of a 2 cm$\times$2 cm area centered at the constriction for several values of L. In all cases, the channel walls seem to squeeze the central intensity peak that slightly penetrates the rectangular billiards through both open endings of the channel. The corresponding calculated frequencies exhibit small fluctuations around 7.74 GHz, as shown in Fig. 15, thus indicating a weak, if any, dependence on L. These fluctuations might as well be due to the variations in the discretization mesh used in each case. Notice that we have kept the number of nodes N in each calculation and chosen some values of L for which the mesh visually had the same channel geometry, as the one shown in Fig. 8. On the other hand, as indicated by the lower panel of Fig. 13 and by the inset in Fig. 15, the channel width W seems to play an important role in the frequency quantization, given the qualitative features that bear resemblance to Fabry-Perot-like resonances in the transverse direction.

Mushroom, cardioid, and irrational triangle billiards. We conclude this paper by applying the numerical method to three distinct geometries recently investigated. Mushroom billiards have been introduced by Bunimovich[28] as the first Hamiltonian systems with a divided phase space (regular and chaotic regions) for which a rigorous mathematical analysis is possible, thus stimulating further studies that include their quantum counterparts. Barnett and Betcke[29] recently reported numerical results for quantum mushrooms using a highly efficient mesh-free boundary method. In their case, for instance, 77 higher-order eigenmodes of a desymmetrized billiard could be numerically calculated within 20 min with a 2.4-GHz CPU. By using a mesh with $N\sim$41000 nodes, we have been able to calculate approximately 10 eigenmodes of a symmetric billiard within 30 min. Some results are shown in Figs. 16 and 17 for a mushroom with a hat of radius R =13.5 cm, and a rectangular foot with height h=23.0 cm and width $2r$=10.0 cm. Figure 16 shows the first ten eigenmodes and Fig. 17 higher-order ones. Interesting sets of odd and even EFs are found, including whispering gallery modes localized in the hat and bouncing ball states in the foot. The cardioid billiard has been investigated recently by Bäcker,[30] who also used a boundary method programmed with the Python language. This billiard has a challenging symmetric geometry with a sharp internal tip in the cavity boundary. Here we consider the ordinary cardioid given in polar coordinates by $r=2(1-\cos\phi)$. A mesh with $N\sim$151000 nodes provided a reasonable discretization around the origin and 20 EFs could be obtained within $T\sim$3 h. Four of them, two odd and two even (with respect to the horizontal symmetry axis), are shown in Fig. 18. Let us finally consider the triangular billiard. In general, plane polygonal billiards have a rich classical dynamics. When all their angles are rational with π, they have long been called "pseudointegrable" by Richens and Berry,[31] because their phase flow is not confined to a

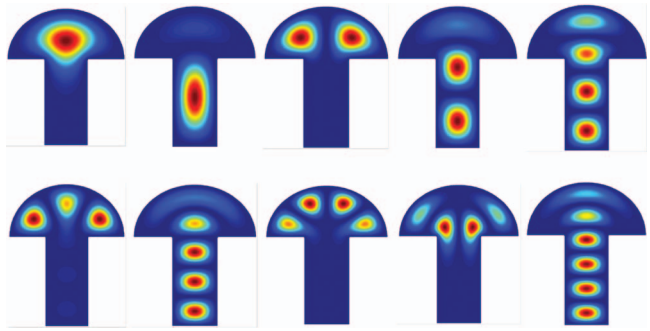

FIG. 16. (Color) Density plots of $|E_z(x,y)|^2$ for the first ten eigenfunctions in a mushroom billiard with a hat of radius R=13.5 cm and a rectangular foot with height h=23.0 cm and width $2r$=10.0 cm. Upper panels, left to right: f=1.2120, 1.6082, 1.7916, 1.8472, and 2.1336 GHz. Lower panels, left to right: f=2.2587, 2.4716, 2.6792, 2.8032, and 2.8363 GHz.

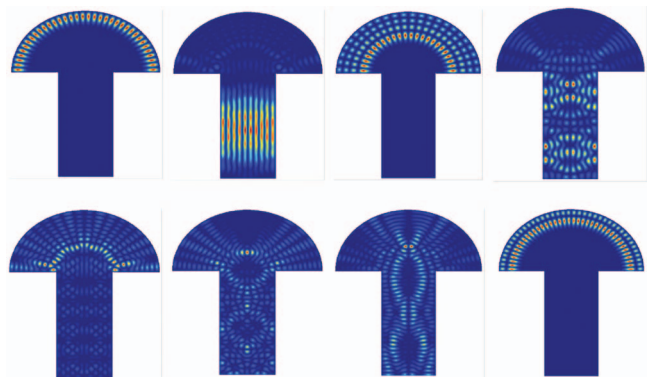

FIG. 17. (Color) Higher-order modes in the same mushroom billiard of Fig. 16. Upper panels, left to right: f=15.0781, 15.0824, 15.1036, and 15.1173 GHz. Lower panels, left to right: f=18.4673, 18.4833, 18.5037, and 18.5291 GHz.

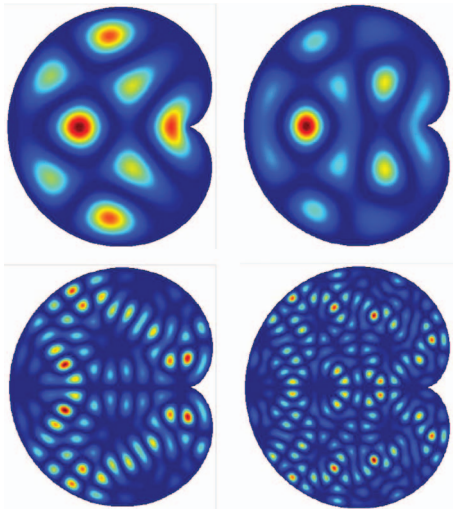

FIG. 18. (Color) Eigenstates of the cardioid billiard: Upper panels: Even modes at $k^2=10.2323$ (left) and 14.4218 (right). Lower panels: Odd modes at $k^2=98.8076$ (left) and 200.7974 (right).

torus. Instead, their classical trajectories cover surfaces for which no unique action variables can be defined. Thus, the motion of a classical particle in such a billiard cannot be integrated. In addition, they have also shown that in quantum mechanics these systems exhibit level repulsion, a feature shared with chaotic billiards.[2] Contrary to previous belief in the mathematical community,[32] Casati and Prosen[33] presented numerical evidence for mixing in triangular billiards when all angles are irrational to π. We numerically quantized a particular acute triangular billiard and some interesting eigenstates are shown in Fig. 19. They exhibit a similar pattern that (i) might be associated with a family of periodic orbits that strongly *diffract* at the upper corner and diffusively *scar* the state, and (ii) does not seem to disappear at large EV orders. Whether such EFs are related to classical *ghosts*[34] or to *superscars*[35] is an issue of ongoing investigations. A detailed analysis that also includes the level dynamics will be published elsewhere.[36]

In sum, we have applied a recent mesh generation technique to a standard finite-element method to numerically solve the eigenvalue problem posed by the Helmholtz equation that describes the wave mechanics in chaotic billiards. The numerical approach provides reasonably fast, relatively cheap, and excellent results as compared to measurements in two-dimensional microwave cavities with different nonintegrable geometries. Its versatility is further demonstrated through calculations in parametric billiards with threefold symmetry and pseudointegrable billiards. In addition, possible localization patterns were identified in a system comprised of two Sinai billiards with accidental degeneracies, coupled through a narrow and short waveguide. Type-II half-filling localization is shown to occur naturally in the coupled system as a result of accidental degeneracies and symmetry, bearing resemblance to a superposition of even-odd partners of a single uncoupled billiard.[6(c)] We report scarred wave functions with a corresponding periodic orbit through the coupling channel that lead to strong localization at the constriction, with eigenfrequencies in the neighborhood of an integer number of $c/2W$, where W is the channel width. In the context of mesoscopic systems, it might be of interest to explore the question of whether such localized states could play a role in the highly nonperiodic electron addition spectrum of two coupled quantum dots, in the low-density regime.[37] Application of the method to study the level statistics in billiards and its possible extension to approach open quantum systems are works underway.

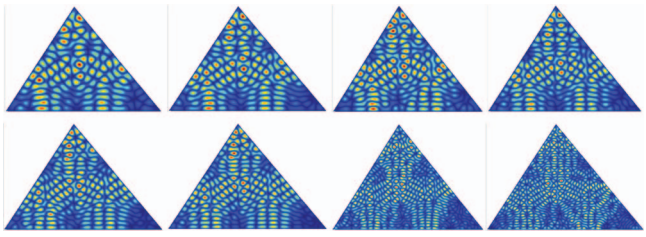

FIG. 19. (Color) Standing-wave patterns in "irrational" (to computer precision) triangular billiard: "superscars" (Ref. 35) or scarred by "classical ghosts" (Ref. 34). The eigenmode order is, left to right, top to bottom, $n=185$, 228, 253, 278, 333, 362, 810, and 998.

We are indebted to the authors of Ref. 21 for making available the mesh generation code that paved most of the way for this work. We thank A. M. S. Macedo and J. R. Rios Leite for stimulating discussions. Professor A. Richter is gratefully acknowledged for information on experiments in microwave billiards made by his group. We would like to thank the referees for bringing Refs. 29, 30, and 38, which propose efficient boundary methods to compute highly excited states of quantum billiards, to our attention. This work has been supported by CNPq and FACEPE, Brazilian Agencies.

[1](a) M. Gutzwiller, *Chaos in Classical and Quantum Mechanics* (Springer-Verlag, New York, 1990); (b) A. M. Ozorio de Almeida, *Hamiltonian Systems: Chaos and Quantization* (Cambridge University Press, Cambridge, UK, 1990); (c) F. Haake, *Quantum Signatures of Chaos*, 2nd ed. (Springer-Verlag, Berlin, 2006); (d) H.-J. Stöckmann, *Quantum Chaos* (Cambridge University Press, Cambridge, UK, 1999).
[2]O. Bohigas, M. J. Giannoni, and C. Schmit, Phys. Rev. Lett. **52**, 1 (1984).
[3]M. L. Mehta, *Random Matrices*, 3rd ed. (Elsevier, Amsterdam, 2004).
[4]E. J. Heller, Phys. Rev. Lett. **53**, 1515 (1984).
[5](a) H.-J. Stöckmann and J. Stein, Phys. Rev. Lett. **64**, 2215 (1990); (b) J. Stein and H.-J. Stöckmann, *ibid.* **68**, 2867 (1992).
[6](a) S. Sridhar, Phys. Rev. Lett. **67**, 785 (1991); (b) S. Sridhar, D. O. Hogenboom, and B. A. Willemsen, J. Stat. Phys. **68**, 239 (1992); (c) S. Sridhar and E. J. Heller, Phys. Rev. A **46**, R1728 (1992).
[7]H.-D. Gräf, H. L. Harney, H. Lengeler, C. H. Lewenkopf, C. Rangacharyulu, A. Richter, P. Schardt, and H. A. Weidenmüller, Phys. Rev. Lett. **69**, 1296 (1992).
[8]C. M. Marcus, A. J. Rimberg, R. M. Westerwelt, P. F. Hopkins, and A. Gossard, Phys. Rev. B **48**, 2460 (1992); F. Simmel, D. Abusch-Magder, D. A. Wharam, M. A. Kastner, and J. P. Kotthaus, *ibid.* **59**, R10441 (1999).
[9]N. Friedman, A. Kaplan, D. Carasso, and N. Davidson, Phys. Rev. Lett. **86**, 1518 (2001).
[10](a) K. K. Huang, Y. F. Chen, H. C. Lai, and Y. P. Lan, Phys. Rev. Lett. **89**, 224102 (2002); (b) T. Harayama, P. Davis, and K. S. Ikeda, *ibid.* **90**, 063901 (2003).
[11](a) R. Blümel, I. H. Davidson, W. P. Reinhardt, H. Lin, and M. Sharnoff, Phys. Rev. A **45**, 2641 (1992); (b) P. A. Chinnery and V. F. Humphrey, Phys. Rev. E **53**, 272 (1996).
[12]C. Ellegaard, T. Guhr, K. Lindemann, H. Q. Lorensen, J. Nygård, and M. Oxborrow, Phys. Rev. Lett. **77**, 4981 (1996).
[13]E. J. Heller, M. F. Crommie, C. P. Lutz, and D. M. Eigler, Nature **369**, 464 (1994).
[14]J. B. Keller, SIAM Rev. **27**, 485 (1985).

[15]P. ŠSeba, Phys. Rev. Lett. **64**, 1855 (1990).
[16]R. J. Riddel, J. Comput. Phys. **31**, 21 (1979).
[17]D. L. Kaufman, I. Kosztin, and K. Schulten, Am. J. Phys. **67**, 133 (1999).
[18]J. Jin, *The Finite Element Method in Electromagnetics*, 2nd ed. (Wiley, New York, 2002).
[19]B. Dietz, A. Heine, V. Heuveline, and A. Richter, Phys. Rev. E **71**, 026703 (2005).
[20]V. Heuveline, J. Comput. Phys. **184**, 321 (2003).
[21]P.-O. Persson, "Mesh generation for implicit geometries," Ph.D. thesis, MIT (2005). Codes currently available from www-math.mit.edu/~persson/mesh/
[22]C. Dembowski, H.-D. Gräf, A. Heine, R. Hofferbert, H. Rehfeld, and A. Richter, Phys. Rev. Lett. **84**, 867 (2000).
[23](a) C. Dembowski, H.-D. Gräf, A. Heine, H. Rehfeld, A. Richter, and C. Schmit, Phys. Rev. E **62**, R4516 (2000); (b) C. Dembowski, B. Dietz, H.-D. Gräf, A. Heine, F. Leyvraz, M. Miski-Oglu, A. Richter, and T. H. Seligman, Phys. Rev. Lett. **90**, 014102 (2003).
[24]H. Alt, H.-D. Gräf, H. L. Harney, R. Hofferbert, H. Lengeler, A. Richter, P. Schardt, and H. A. Weidenmüller, Phys. Rev. Lett. **74**, 62 (1995).
[25]F. Leyvraz, C. Schmit, and T. H. Seligman, J. Phys. A **29**, L575 (1996).
[26]A. Richter (private communication).
[27]D. Rolles, M. Braune, S. Cvejanovic, O. Gessner, R. Hentges, S. Korica, B. Langer, T. Lischke, G. Prümper, A. Reinköster, J. Viefhaus, B. Zimmermann, V. McKoy, and U. Becker, Nature **437**, 711 (2005).
[28]L. A. Bunimovich, Chaos **11**, 802 (2001).
[29]A. H. Barnett and T. Betcke, preprint arXiv:nlin.CD/0611059 (2006).
[30]A. Bäcker, Lect. Notes Phys. **618**, 91 (2003).
[31]P. J. Richens and M. V. Berry, Physica D **2**, 495 (1981).
[32]E. Gutkin, J. Stat. Phys. **83**, 7 (1996).
[33]G. Casati and T. Prosen, Phys. Rev. Lett. **83**, 4729 (1999).
[34]P. Bellomo and T. Uzer, Phys. Rev. A **51**, 1669 (1995).
[35]E. Bogomolny and C. Schmit, Phys. Rev. Lett. **92**, 244102 (2004).
[36]F. M. de Aguiar and D. D. de Menezes (unpublished).
[37]M. Brodsky, N. B. Zhitenev, R. C. Ashoori, L. N. Pfeiffer, and K. W. West, Phys. Rev. Lett. **85**, 2356 (2000).
[38]G. Veble, T. Prosen, and M. Robnik, preprint arXiv:nlin.CD/0612011 (2006).